Picosecond polarization-selective transient grating experiments in sodium-seeded flames

John T. Fourkas, Timothy R. Brewer, Hackjin Kim, and M. D. Fayer
Department of Chemistry, Stanford University, Stanford, California 94305

(Received 2 May 1991; accepted 11 July 1991)

Polarization-selective transient grating experiments have been used to study the subnanosecond time scale dynamics of several sodium-seeded, premixed flames. Intensity gratings (in which both excitation beams are of the same polarization) were used to determine excited-state quenching collision rates, while polarization gratings (in which the excitation beams are cross polarized) were used to measure Na diffusion constants and the rates of Na ground state magnetic sublevel population scattering collisions. In addition, the rates of scattering between the $3P_{1/2}$ and $3P_{3/2}$ excited state levels were measured using an excited state probing scheme.

I. INTRODUCTION

Combustion is an extremely complex process, with hundreds of chemical reactions taking place in flames of even the simplest of fuel/oxidant mixtures.[1] Furthermore, the dominant chemical processes in a flame can vary greatly from region to region. These regions communicate with each other through transport and collisions. Thus it is desirable to develop noninvasive techniques that can probe the dynamic properties of a flame (e.g., diffusion rates, collision rates, and velocity distributions) over small distance scales and on short (subnanosecond) time scales.

Due to their noninvasive nature, various spectroscopic methods have become popular combustion diagnostics in recent years. However, these techniques have found their greatest use in measuring relatively slowly varying or "static" flame properties, such as species concentrations and temperatures. Laser techniques such as coherent anti-Stokes Raman scattering (CARS),[2,3] laser induced fluorescence (LIF),[4,5] and frequency-domain four-wave mixing (FWM)[6-10] have provided temperature and concentration information on various flame species. In addition, all of the above methods can be used to image concentrations of flame species.

Each of the aforementioned techniques has desirable properties; the signal may be spatially separate from the laser beams (CARS and FWM), of a different frequency than some or all of the laser beams (LIF, CARS, and FWM), and/or of a different polarization than some or all of the laser beams (FWM). As useful as these techniques are, however, none of them measures fast dynamic combustion processes directly and unambiguously. In order to probe such processes, it is necessary to perform time-domain experiments using subnanosecond laser pulses. The transient grating[11] (TG) combines the advantages of the above techniques with picosecond or femtosecond laser pulses, thus providing a useful method for studying ultrafast combustion dynamics over small distance scales. We have reported the preliminary results of picosecond, polarization-selective TG studies of sodium atom dynamics in a Na-seeded, premixed, methane/air flame.[12] Here we present detailed results of our studies of several premixed flames.

II. BACKGROUND

The transient grating is a time-domain FWM experiment. Two time-coincident laser pulses of the same wavelength (λ) are crossed at an angle θ in a sample, thereby creating a sinusoidal interference pattern of fringe spacing $d = \lambda/[2\sin(\theta/2)]$ in the overlap region [Fig. 1(a)]. If the

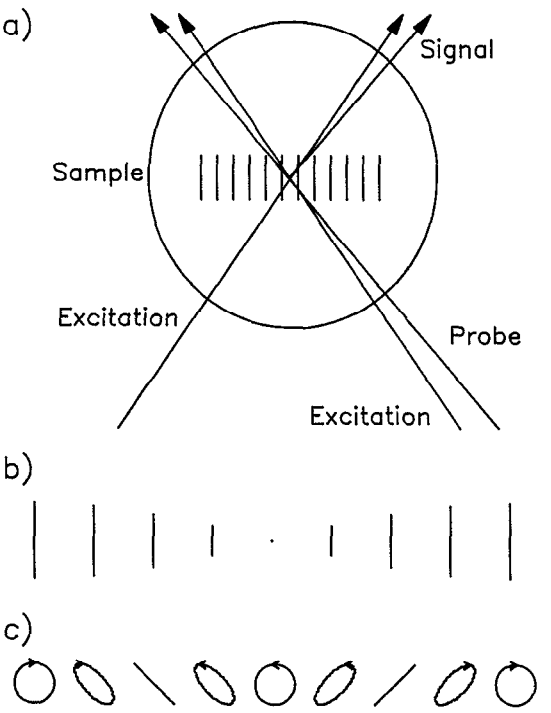

FIG. 1. (a) Transient grating experimental geometry. The excitation beams are spatially and temporally overlapped, and therefore create a spatial interference pattern that writes a grating into the sample. The probe beam approaches the grating to meet the Bragg condition, and part of this beam is diffracted to create the signal beam. (b) Electric field picture for one fringe of an intensity grating. The electric field amplitude varies sinusoidally across each fringe, but the polarization remains the same. (c) Electric field picture for one fringe of a polarization grating. The electric field amplitude is constant across each fringe, whereas the polarization changes from rcp to linear at $-45°$ to lcp to linear at $+45°$.

 0021-9606/91/205775-10$03.00

laser beams are resonant with an electronic transition in the sample, the interference pattern produces a spatial grating in the excited state population (and a corresponding grating in the ground state population). Excitation beams of parallel linear polarizations form a linear intensity grating. The light electric field is of the same polarization throughout this grating [Fig. 1(b)], and so a spatial modulation in the amount of excited state population is produced. Cross-polarized excitation beams form a linear polarization grating, which has a more complicated spatial electric field dependence.[13,14] The electric field is of equal amplitude throughout the grating, but changes from right circularly polarized (rcp) to linear at $-45°$ to left circularly polarized (lcp) to linear at $+45°$ and back to rcp over each fringe spacing [Fig. 1(c)]. Thus the excited state population is uniform in magnitude but not in its manner of preparation across each fringe (as opposed to the intensity grating, in which the excited state population is uniform in manner prepared but not in magnitude across each fringe).

Some time after the grating is created, it is probed with a third laser pulse. This pulse may be resonant with the same ground state-excited state transition, a different ground state-excited state transition, or an excited state-excited state transition. The probe beam approaches the overlap region from just above one of the excitation beams (such that it meets the Bragg condition but is spatially separate from the excitation beams), and a portion of it diffracts off of the grating; the signal beam emerges just below the other excitation beam [Fig. 1(a)]. Processes such as excited state decay, species transport, and internal population transfer can wash out the grating; thus the dependence of the signal amplitude on the delay between creating and probing the grating is a sensitive probe of these effects. Rose *et al.* have analyzed TG decays of gas-phase systems in two regimes, free and diffusive transport.[15,16] In the free transport regime, in which the mean free path (along the grating wavevector) of the atom or molecule being probed is much greater than the grating fringe spacing, the signal is given by

$$S(t) \propto \exp[-(\Delta t)^2 k_B T/m]\exp[-2t/\tau], \qquad (1)$$

where t is the delay time, Δ is $2\pi/d$, k_B is Boltzmann's constant, T is the temperature, m is the mass of the atom or molecule, and τ is the excited state lifetime. In the diffusive transport regime, in which the mean free path of the species being probed is much less than the fringe spacing, the signal is given by

$$S(t) \propto \exp[-2(\Delta^2 D + 1/\tau)t], \qquad (2)$$

where D is the diffusion constant of the atom or molecule. Experiments can be done in both of these regimes in flames, but we will concentrate here on the diffusive regime. Note that both of the above equations are for effective two-state systems. It is also assumed in these equations that no population is scattered to other states; corrections for such scattering will be added where appropriate below.

We report the results of TG studies of sodium atom diffusion rates, excited-state quenching rates, ground state magnetic sublevel population scattering rates, and excited-state population scattering rates in various premixed flames. Although Na is not intrinsic to most flames, it is often used to test new combustion diagnostics. This is because the physics of the Na atom is well understood, the Na $3s$–$3p$ transitions are strong and at a convenient wavelength, and Na is readily introduced into a flame in controllable quantities. For instance, Ewart *et al.* have demonstrated fluorescence imaging and broadband FWM,[6,7] Kneisler *et al.* have demonstrated a pump–probe technique,[17] and Trebino and Rahn have studied collision-induced four- and six-wave mixing spectra in Na-seeded flames.[18,19] In addition, TG experiments have been performed on gas-phase Na atoms in a low-pressure cell by Rose *et al.*[15,16]

As we will show in the theory section of this paper, the Na TG decays we have observed can be explained completely in terms of the dynamics of Na atoms in the flame and the behavior of the magnetic sublevels of the hyperfine levels of the Na atoms. The energy level diagram for the Na $3s$ and $3p$ levels is shown in Fig. 2. Spin–orbit coupling splits the $3p$ orbital into the $P_{1/2}$ and $P_{3/2}$ levels, which are separated by 17 cm^{-1}. All of the levels are further split by coupling with the nuclear spin of $I = 3/2$. The $3s$ orbital is split into $F = 1$ and $F = 2$ hyperfine levels, which are separated by 1.77 GHz. The $P_{1/2}$ level is split into $F = 1$ and $F = 2$ hyperfine levels and the $P_{3/2}$ level is split into $F = 0$, 1, 2, and 3 hyperfine levels; all of the $3p$ hyperfine splittings are at least an order of magnitude smaller than the ground state splitting. Finally, each of the hyperfine levels has $2F + 1$ magnetic sublevels with quantum numbers $m_F = -F$ to F.

III. EXPERIMENTAL PROCEDURE

The experimental setup is shown in Fig. 3. A frequency-doubled, acousto-optically Q-switched and mode-locked Nd:YAG laser was used to synchronously pump two independently tunable, cavity-dumped dye lasers at a repetition

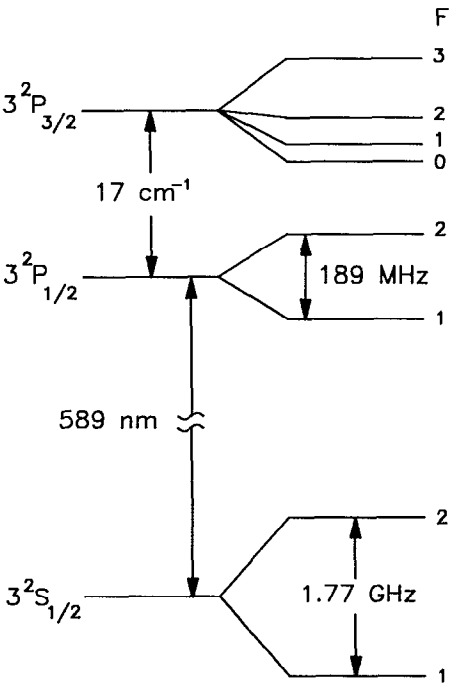

FIG. 2. Energy level diagram for Na $3s$ and $3p$ orbitals.

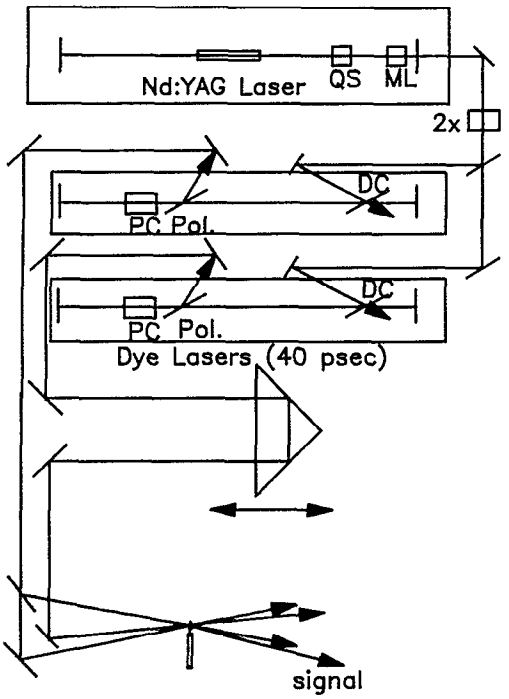

FIG. 3. Experimental setup. A frequency-doubled, acousto-optically Q-switched and mode-locked Nd:YAG laser is used to synchronously pump two independently tunable dye lasers. One dye laser is used to make the excitation beams, which are split and recombined in the flame. The output of other dye laser is sent down an optical delay line and is the used to probe the grating formed by the excitation beams. PC = Pockel's cell, Pol = polarizer, ML = mode-locker, QS = Q-switch, DC = dye cell.

rate of 1 kHz. The dye lasers produce 10 μJ, 40 ps (FWHM) pulses with a bandwidth of about 0.9 cm^{-1}. The excitation and probe dye lasers may be tuned to the same or to different Na D lines [$\lambda(D_1) = 589.6$ nm, $\lambda(D_2) = 589.0$ nm]; the lasers are usually tuned to different D lines so that the scattered light from the excitation beams can be filtered out. The output of one dye laser is split to form the two excitation beams, which are then crossed in the flame to make the grating. The output of the other dye laser is sent down an optical delay line, and then the beam is diffracted off of the grating. All three beams are attenuated to about 100 nJ before they enter the flame. The spot sizes ($1/e$ diameter) are 180 μm for the excitation beams and 140 μm for the probe beam (although spots smaller than 50 μm can be readily employed). In order to cut down on background light from the flame and scattered light from the laser beams, the signal beam passes through two irises, an etalon, and a polarizer. The signal is detected with a phototube and a gated integrator. A computer monitors the output from both the gated integrator and a reference photodiode (which monitors the shot-to-shot laser intensity). The computer only records data from shots for which the sum of twice the excitation beam intensity plus the probe beam intensity is within a 10% window (this intensity ratio accounts for the different effects of excitation and probe beam fluctuations on the grating signal).

The burner used in the experiment is a Perkin–Elmer atomic absorption burner with a 10.4 cm long, 0.7 mm wide slot. To ensure a constant flow of Na into the burner (which is important for a good signal-to-noise ratio, since the signal is proportional to the square of the Na concentration), a 0.26 M NaCl solution is pumped (rather than aspirated) into the burner, at the rate of 1.1 ml/min. Initially, a near-stoichiometric methane/air flame was investigated. All experiments were performed 13 mm above the burner slot and about 3 mm above the flame front of each flame.

To ensure that the same spot was probed at each fringe spacing, before each experimental run the laser beams were aligned through a pinhole assembly that fits into the burner slot. The pinhole assembly was then removed and the burner turned on and allowed to warm up for at least 10 min, including at least five in which the NaCl solution was flowing. The laser wavelengths were tuned by passing the beams through a low-pressure Na cell and monitoring the resultant fluorescence. The beams were then retuned in the flame to maximize the observed signal at a delay time much longer than the laser pulse durations.

IV. RESULTS AND DISCUSSION

Intensity and polarization grating data were taken at 15 fringe spacings in the methane/air flame. Figure 4(a) shows a sample intensity grating data set taken at a fringe spacing of 13.6 μm; the excitation laser was tuned to the D_1 line and the probe laser was tuned to the D_2 line. The decay is essentially exponential (except for a spike at early time due to coherence effects when all of the laser beams are temporally overlapped, and other early time effects that will be discussed later), with a signal decay time of 0.4 ns (corresponding to a 0.8 ns decay constant). This decay time is much shorter than the natural 16 ns Na excited state lifetime.[20]

Figure 4(b) shows a polarization grating decay taken at the same fringe spacing. The differences between the two decays are striking; the polarization grating decay has an exponential envelope and shows large oscillations at the ground state hyperfine splitting frequency (as well as smaller oscillations at twice the ground state hyperfine splitting frequency). Note that, due to collisional and Doppler broadening, this 1.77 GHz ground-state hyperfine splitting is too small to be observed in an absorption spectrum taken in the same flame, yet it is readily apparent in the polarization grating decay. Although the envelope of this decay is exponential, the decay time is 2.8 ns (corresponding to a 5.6 ns decay constant), which is about seven times slower than the decay of the intensity grating at this fringe spacing. Furthermore, intensity grating decays are insensitive to fringe spacing over the range of fringe spacings studied (from 5 to 22 μm), suggesting that the dominant decay mechanism is collisional quenching of the Na excited states (and not transport). On the other hand, the polarization grating decays change significantly with fringe spacing, because there is time for diffusion to influence the decay.

Figure 5 is a plot of the polarization grating envelope decay constant vs Δ^2. This plot is consistent with decays that are dominated by diffusion as per Eq. (2), and gives a diffusion constant of 4.3 cm^2/s. This number is in good agreement with previous measurements made by Ashton and Hayhurst[21] on a millimeter distance scale. The TG experiment, however, can measure diffusion over a much shorter

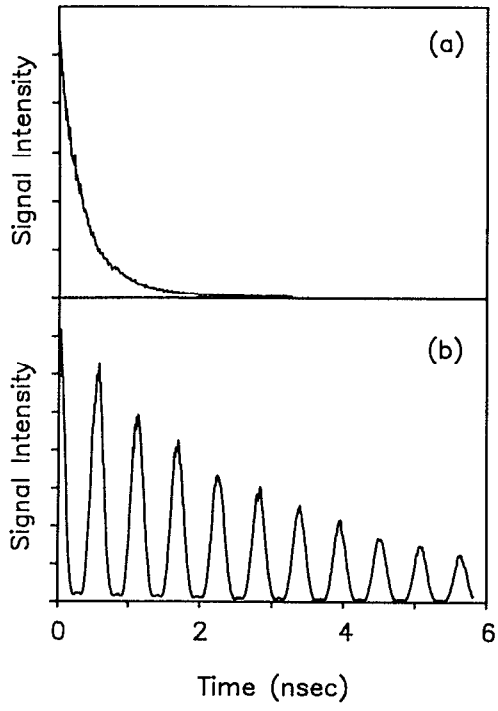

FIG. 4. (a) Intensity grating decay in methane/air flame (fringe spacing 13.6 μm, $\lambda_{exc} = 589.6$ nm, $\lambda_{probe} = 589.0$ nm). The decay is exponential after short delay times, with a decay time of 400 ps. (b) Polarization grating decay in the same flame at the same fringe spacing. The envelope of the decay is exponential, with a decay time of 2.8 ns, about seven times longer than the intensity grating decay. In addition, the polarization grating decay shows large oscillations at the Na ground state hyperfine splitting frequency, 1.77 GHz, as well as small beats at twice this frequency.

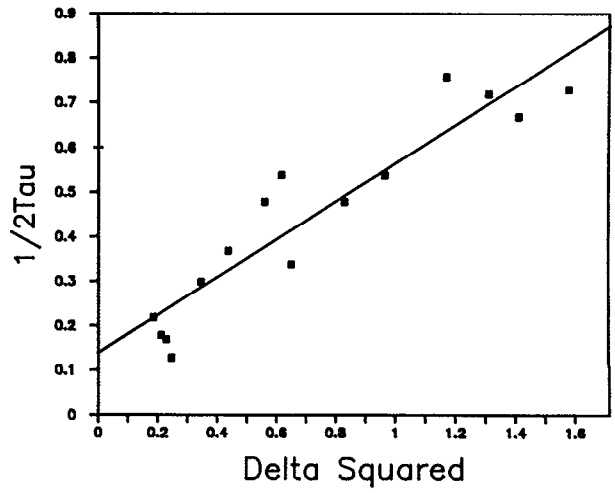

FIG. 5. Polarization grating decay constant vs Δ^2 in the methane/air flame. The slope of the plot gives the Na diffusion constant (D) and the intercept gives the rate of collisions that scatter population among the ground state magnetic sublevels.

range. The TG is sensitive to transport on the distance scale of one fringe spacing, and the laser spot size determines how large a region is probed. The fringe spacing can be as small as half of the wavelength of the light used (well less than 0.5 μm), and it is desirable to have at least ten fringes within the grating volume to get reasonable diffraction efficiency. Thus it is possible to measure transport over distances of less than a micron in a spot less than 50 μm in diameter in a TG experiment.

Note also that the y intercept of the plot in Fig. 5 is not zero. In fact, it corresponds to a decay process that has a 6 ns lifetime; this lifetime is different from both the 0.8 ns excited state quenching time and the 16 ns natural excited state lifetime. As we will show below, this decay is due to scattering of population among the ground state magnetic sublevels; to our knowledge, this scattering rate has never before been directly measured before in a flame. The formal details of the behavior of both the intensity and polarization grating decays will be explained in Sec. V.

The intensity grating decay is due to collision-induced excited-state quenching. The 0.8 ns decay time that we have measured is in reasonable agreement with the results of previous investigators. Russo and Hieftje measured a 0.48 ns quenching time in a natural-gas/air flame using optoelectronic cross-correlation.[22] Takubo *et al.* used time-correlated single-photon counting to measure a 0.69 nsec quenching time in a propane/air flame.[23] Using on-the-fly, gated single-photon counting, Alfano measured a 0.56 ns quenching time in a methane/nitrogen/oxygen flame and a 1.1 ns quenching time in a methane/argon/oxygen flame.[24] Finally, Kneisler *et al.* used a pump–probe technique to measure a 1.2 ns quenching time in a methane/air flame.[17] The time resolution of the TG experiments reported here is comparable to or better than that in the experiments of the other investigators. The TG has the additional advantages of being a background-free experiment and being much less sensitive to reabsorption than the experiments mentioned above; thus, it is possible to achieve a much higher signal-to-noise ratio in a TG experiment. It should also be noted that none of these investigators reported at what spot in the flame their measurements were made, and that the quenching constant would be expected to change with different flame compositions.

In order to learn more about the Na excited state quenching agent or agents, data were taken in three other near-stoichiometric flames: hydrogen/air, methane/argon/oxygen, and hydrogen/argon/oxygen. (In the latter two flames, the argon and oxygen were in a 4:1 molar ratio.) In each flame, the data were taken at six fringe spacings from 5.3 to 13.2 μm. This was enough data points to determine the slope of the decay time vs Δ^2 plots, but not enough to determine the intercept very precisely. The diffusion constants and quenching times for these flames are listed in Table I. It should be noted that because the flames burn at different temperatures, the diffusion constants and quenching times are not directly comparable, but rather serve to show trends. However, in each flame the flow rates of the gases were chosen such as to make the flame front sit the same distance above the burner head; in addition, the data were taken the same distance above each flame front.

Molecular nitrogen is known to be an efficient quencher of Na excited states.[25] However, as can be seen in Table I, the quenching time only increased by 50% in going from the methane/air to the methane/argon/oxygen flame. Carbon

TABLE I. Quenching times, diffusion constants, and excited state scattering rates.[a]

	Quenching time τ_q (ns)	Diffusion constant D (cm^2/s)	Excited state scattering rate k_d (10^9/s)
Methane/air	0.8(1)	4.3(5)	1.6(3)
Methane/Ar/O_2	1.2(1)	5.5(7)	2.2(4)
H_2/air	0.8(1)	4.4(6)	2.2(4)
H_2/Ar/O_2	1.0(1)	5.6(6)	2.6(4)

[a] Numbers in parentheses are uncertainty in the last digit.

dioxide is also an especially efficient Na excited-state quencher,[25] but the quenching times in the hydrogen flames are quite similar to those in the methane flames. This suggests that carbon-containing species are not especially important in the quenching reactions. There are three possible explanations for the relative insensitivity of the quenching rate to the composition of the flame: (1) The major quenching species are composed of oxygen and/or hydrogen; (2) there are so many efficient quenchers in the flame that removing N_2 has little effect on the total quenching rate; (3) so much N_2 is entrained into the flame from the surrounding atmosphere that removing N_2 from the oxidant mixture has only a minor effect on the quenching rate. It seems probable that the answer is a combination of all three explanations.

There are several other processes that could affect the decay of the intensity grating and that therefore should be considered. For example, the decays could be affected by state-dependent ionization. If the ionization rate of excited Na atoms is faster (or slower) than the ionization rate of ground state Na atoms, and if the faster of the two ionization rates is not negligible compared to the excited state quenching rate, then quenching will not completely destroy the grating. Higher excited states of Na are known to have accelerated ionization rates in flames; however, the difference in rates between atoms in the ground state and in the first excited state is minuscule.[26] Furthermore, state-selective ionization would add a slow, diffusional component to the intensity grating decay, and we have not observed any such slow decay component at any fringe spacing.

Scattering of population between the $3P_{1/2}$ and $3P_{3/2}$ excited state levels can affect the grating decay. We will show below that this is not an important effect if the decays are fit starting at a long enough delay time. Finally, the grating decays also might be affected by high Na densities or by contributions from other species in the flame. However, the observed grating decay times were independent of Na concentration over the wide range of concentrations tested. In addition, no TG signal was seen in the absence of Na.

By using excited state probing, it is also possible to measure the rate of scattering of population between the $3P_{1/2}$ and $3P_{3/2}$ states. To calculate how this scattering would affect the grating signal in such an experiment, we start by assuming that the dominant kinetic processes in the experiment are excited state relaxation and scattering of population between the $3p$ levels. This is a reasonable assumption since (1) The 17 cm^{-1} splitting between the $3p$ levels is much smaller than the energy difference between the $3p$ levels and any other excited state levels; (2) there are no energy levels between the ground state and the excited states monitored; and (3) the equilibrium population of the $3s$ energy level is many orders of magnitude greater than the equilibrium population of the $3p$ states at around 2000 K. We can thus write coupled equations for the time-dependent populations of the $3p$ levels:

$$\frac{-d[1/2]}{dt} = k_r[1/2] + k_u[1/2] - k_d[3/2],$$
$$\frac{-d[3/2]}{dt} = k_r[3/2] + k_d[3/2] - k_u[1/2], \tag{3}$$

where $[1/2]$ and $[3/2]$ are the populations of the $3P_{1/2}$ and $3P_{3/2}$ states respectively, k_r is the excited state relaxation rate, k_d is the scattering rate from the $3P_{3/2}$ level down to the $3P_{1/2}$ level, and k_u is the scattering rate from the $3P_{1/2}$ level up to the $3P_{3/2}$ level (see Fig. 6). From detailed balance we find that $k_u = 2k_d$ at infinite temperature; at the temperatures of the flames investigated, this number is closer to 1.96, but we will approximate it as 2 for convenience in our analysis. We can now solve these coupled equations for an experiment in which the excitation is made to the $3P_{1/2}$ level ($[1/2] = 1$ and $[3/2] = 0$ at $t = 0$). We find that

$$[1/2] = (1/3)\exp(-k_r t)[1 + 2\exp(-3k_d t)],$$
$$[3/2] = (2/3)\exp(-k_r t)[1 - \exp(-3k_d t)]. \tag{4}$$

The best experimental configuration for measuring the excited state scattering rate is to probe a transition from the excited state that is being scattered into (as opposed to the excited state to which the excitation was made) to a higher excited state. This arrangement has the dual advantages of probing at a wavelength that is quite different from the excitation wavelength (such that scattered light from the excitation

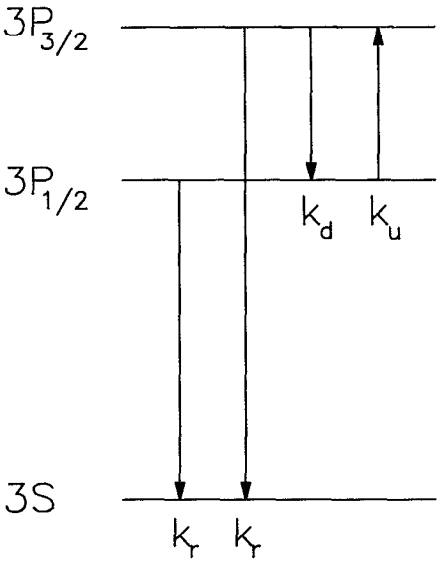

FIG. 6. Kinetic scheme for important population-scattering processes in the Na atom. The rate of excited-state relaxation, through fluorescence and quenching, is k_r. The rate of scattering from the $3P_{1/2}$ to the $3P_{3/2}$ is k_u, and the rate for the opposite process is k_d. These two rates are related at infinite temperature by $k_u = 2k_d$.

beams can be removed) and not having a coherence spike in the decay (because the state being probed is not coherently coupled to the ground state). The Na $3P_{3/2}$–$4D$ transition is an ideal probe transition in such an experiment, as it has a relatively large oscillator strength and its wavelength is 5688 Å. Using Eqs. (4) we find for this experiment that

$$S(t) \propto \exp(-2k_r t)[1-\exp(-3k_d t)]^2. \quad (5)$$

Thus the signal builds in at a rate determined by the excited-state scattering time, and decays at a rate determined by the excited-state quenching time.

This experiment was performed in all four flames. The fringe spacing was made as large as was easily possible (22 μm), so that there would not be any diffusional contribution to the decay. The spot sizes were increased to about 300 μm, so that there would be more than ten fringes in the grating volume. A 10 nm bandwidth interference filter centered at 570 nm was placed in front of the phototube to filter out both scattered light from the excitation beams and any stray doubled-YAG light. A typical data set is shown in Fig. 7(a); this particular set was taken in a hydrogen/argon/oxygen flame. For comparison, Fig. 7(b) shows a decay, taken in the same flame, in which the excitation was from the ground state to the $3P_{3/2}$ level and the probing was from the $3P_{3/2}$ level to the $4D$ level. In this case, the rise time of the signal should be limited only by the width of the laser pulses used. Although the maximum of the data in Fig. 7(b) is obscured somewhat by the small coherence artifact, it can be seen that this signal reaches its maximum before the signal in Fig. 7(a).

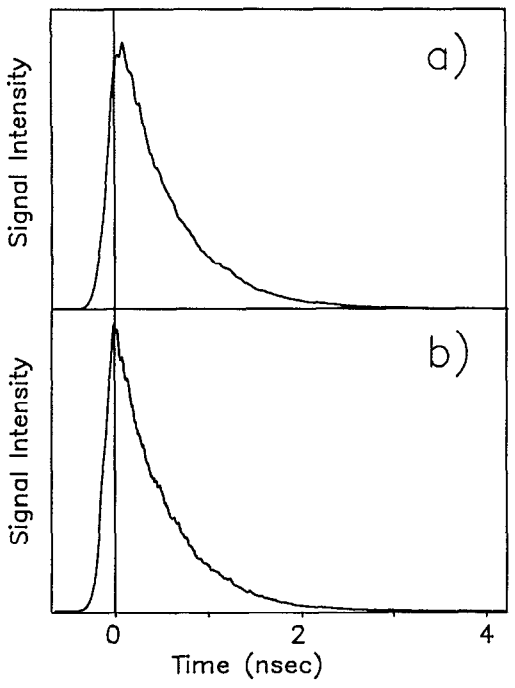

FIG. 7. Excited state probing data in methane/air flame. (a) Decay for excitation from ground state to $3P_{1/2}$ and probing from $3P_{3/2}$ to $4D$. (b) Decay for excitation from ground state to $3P_{3/2}$ and probing from $3P_{3/2}$ to $4D$. The second decay peaks a few hundred picoseconds earlier than the first.

The data for excitation to the $3P_{1/2}$ level and probing from the $3P_{3/2}$ level to the $4D$ level were first fit by squaring the convolution of Eq. (5) with the excitation pulse shape, and then convolving with the probe pulse shape. For the range of excited-state scattering and excited-state quenching rates observed in these experiments, we were able to show that the results of the above convolutions were virtually indistinguishable from the convolution of Eq. (5) with the instrument response function. Since the latter method is faster, it was used to fit all of the data sets. The instrument response was found by taking an optical Kerr effect TG decay in a CS_2 cell and fitting it to a Gaussian. The convolution of these two functions fits the data quite well except in the earliest part of the rising edge, where the signal is sensitive to the slightly non-Gaussian temporal profile of the laser pulses. The measured k_d for the four flames are given in Table I. These values correspond to scattering times from the $3P_{1/2}$ level to the $3P_{3/2}$ level on the order of 0.2 to 0.3 ns, which is somewhat longer than the value previously measured by Takubo *et al.* in a propane/air flame using time-correlated single photon counting.[20] The TG experiment has time resolution comparable to that of the photon-counting experiment and has the great advantage of being background-free; thus the TG should be a more sensitive probe of the excited-state scattering rate.

The excited-state quenching times measured in this experiment were identical (within experimental error) to those measured in the ground state probing experiment. We can use Eqs. (4) to calculate the exact form of the decay in that experiment also (neglecting the coherence spike). The signal is given by the square of the sum of an absorptive component and a stimulated emission component. The absorptive component is proportional to the peak–null population difference in the ground state (or, equivalently, the total excited state population in a peak of the grating). The stimulated emission component is proportional to the population of the excited state being probed from the ground state. Thus we find, for excitation from the ground state to the $3P_{1/2}$ level and probing from the ground state to the $3P_{3/2}$ level:

$$S(t) \propto ([1/2] + 2[3/2])^2$$
$$\propto \exp(-2k_r t)[5 - 2\exp(-3k_d t)]^2. \quad (6)$$

This equation reduces to Eq. (2) at long enough delays, and it is clear from the measured values of k_d that the ground state probing data can be fit using Eq. (2) for delay times greater than a few hundred picoseconds.

It is also interesting to compare the scattering cross sections for the various processes that have been measured. In the hard-sphere limit, the average cross section for diffusional collisions is given by[27]

$$\sigma_D = 2[(k_B T)^3/\pi m]^{1/2}/3pD, \quad (7)$$

where m is the mass of the Na atom and p is the pressure of the flame. The excited state quenching cross section is related to the quenching lifetime, τ_q, by the relation[27]

$$\sigma_q = (\pi\mu k_B T/8)^{1/2}/p_q\tau_q, \quad (8)$$

where μ is the average reduced mass of Na and its quenching-collision partners (we take this number to be one half of

the mass of Na for simplicity), and p_q is the pressure of quenchers. A similar expression can be written for σ_e, the cross section for scattering between the $3P_{1/2}$ and $3P_{3/2}$ excited state levels. Note, however, that we know neither p_q, the pressure of quenchers, nor p_e, the pressure of excited-state scatterers; rather, we know that p_q and p_e can be no larger than 1 atm. Thus only the *minimum* value of these two scattering cross sections can be calculated, by assuming that p_q and p_e are both equal to 1 atm. We assume temperatures of 1800 K for the methane/air flame, 1600 K for the methane/argon/oxygen flame, 2000 K for the hydrogen/air flame, and 1800 K for the hydrogen/argon/oxygen flame.[28] The minimum scattering cross section values and the diffusional collision cross sections are listed for all of the flames in Table II. The uncertainty in each of the cross sections is about ± 0.05 nm^2; this uncertainty arises mostly from not knowing the exact temperatures of the flames at the spots where data were taken.

Inspection of Table II shows that, for a given flame, the diffusional collision cross section is identical to the minimum excited state quenching cross section (within experimental error), and is smaller than the excited-state population scattering cross section. The excited-state quenching cross section must be substantially larger than the maximum value, since, in the Ar-containing flames, Ar cannot quench Na. The pressure of quenchers is substantially less than one atmosphere, and the cross section is therefore substantially greater than the minimum value. Therefore neither the quenching nor population-scattering collisions randomize the Na velocity.

V. THEORETICAL RESULTS

Because the energy levels and relative optical transition strengths of the Na atom are well known, it is possible to perform a complete theoretical analysis of the experiments presented here. The Na atom is a multilevel system, and thus the perturbation theory analysis of these experiments is very complex. Therefore we will present only a qualitative discussion of the relevant physics and the results of the perturbation theory calculation in this paper. The detailed theory will be presented elsewhere.[29]

There are two major differences between the intensity and polarization grating decays in the flames: (1) the intesity grating decays are shorter than the polarization grating decays and are insensitive to diffusion, and (2) the intensity gratings decay smoothly whereas the polarization grating decays exhibit beats at the ground state hyperfine splitting frequency. Although Rose *et al.* observed oscillations in Na polarization grating decays in a low-pressure Na cell,[15,16] the differences between the intensity and polarization grating decay times in flames had not been previously predicted theoretically or observed experimentally. Rose *et al.* correctly interpreted the oscillations as arising from coherences created between ground state magnetic sublevels in different hyperfine levels during the formation of the grating.[16] While their mechanism was qualitatively correct, the mathematical treatment did not provide an accurate description of the experiment involved, and it lacked predictive capability. The behavior of atmospheric-pressure (and low-pressure) Na transient grating decays can be fully and quantitatively explained using diagrammatic perturbation theory and the grating decomposition method (GDM). This problem is treated formally and in detail elsewhere.[29] Here we present a summary of the results.

TABLE II. Hard sphere scattering cross sections (all uncertainties about 0.05 nm^2).

	Diffusion σ_D (nm^2)	Quenching (minimum) σ_q (nm^2)	Excited state scattering (minimum) σ_e (nm^2)
Methane/air	0.17	0.17	0.22
Methane/Ar/O_2	0.11	0.11	0.28
H_2/air	0.20	0.18	0.30
H_2/Ar/O_2	0.13	0.13	0.37

We first present a qualitative explanation of these experiments. If the polarizations of the excitation beams in a grating experiment are identical, the resultant electric field is of a single polarization and is modulated sinusoidally in amplitude; thus it is straightforward to analyze phenomenologically how processes such as transport and population transfer affect the signal decay. However, when the excitation beams are cross polarized, it is not obvious how to deal with the spatial dependence of the grating electric field. The ability to incorporate spatial information about the excitation process is essential to understanding the decay mechanisms of the Na intensity and polarization gratings. Using the GDM, we can show that polarization grating calculations can be viewed as the sum of calculations of four separate intensity gratings: a rcp grating, a $-45°$ linear grating that is spatially $\pi/2$ radians out of phase with the rcp grating, a lcp grating that is spatially π radians out of phase with the rcp grating, and a $+45°$ linear grating that is spatially $3\pi/2$ radians out of phase with the rcp grating. It is as if each of these component gratings is created with two excitation beams of the same polarization; e.g., the first component grating looks as if it were created by two rcp excitation beams. Thus the problem can be thought of in terms of four separate grating electric fields that vary only in amplitude across each fringe; therefore, spatial information about the excitation and decay processes is readily available. Furthermore, the final grating signal can be calculated by summing, with the proper spatial phases, the contributions of each component grating to the third-order polarization.

To understand how the four component intensity gratings influence the polarization grating signal, it is necessary to consider the selection rules for transitions out of the Na magnetic sublevels: $\Delta m_F = \pm 1$ for x- and y-polarized light, $\Delta m_F = 0$ for z-polarized light, $\Delta m_F = +1$ for rcp light, and $\Delta m_F = -1$ for lcp light. It can be seen from the selection rules for rcp and lcp light and from the fact that the rcp and lcp component gratings are 180° spatially shifted that the polarization grating experiment must involve optical pumping.[30] Consider, for example, how the four component gratings affect transitions from the $|2\ 2\rangle$ ground state magnetic sublevel to the $3P_{1/2}$ excited state manifold. Because

there is no magnetic sublevel with $m_F = 3$ in this excited state manifold, the rcp component cannot drive any transitions at all. On the other hand, the lcp grating, which has a selection rule of $\Delta m_F = -1$, can drive transitions to the $|1\ 1\rangle$ and $|2\ 1\rangle$ magnetic sublevels, as can the $-45°$ and $+45°$ linear component gratings. The $|2\ -2\rangle$ ground state magnetic sublevel behaves in the opposite manner; no transitions are driven by the lcp component grating, whereas the other three component gratings do drive transitions out of this magnetic sublevel. Thus, in these two ground state magnetic sublevels, the polarization grating excitation process effectively creates gratings that are spatially 180° out of phase with one another. Gratings are created in the other ground state magnetic sublevels with nonzero m_F in a similar manner; because magnetic sublevels with an m_F of zero are affected equally by rcp and lcp light, no gratings are formed in these states.

Incorporating these ideas, we are able to calculate the amount of population transferred out of each ground state magnetic sublevel during the excitation steps in both the intensity and the polarization gratings, and thus obtain a qualitative understanding of the decay mechanisms. In an intensity grating, the population transferred from a ground state sublevel varies sinusoidally across the grating, with an amplitude proportional to the sum of the oscillator strengths (at the proper light polarization) to all possible resonant excited state magnetic sublevels. Similarly, we calculate the population transfer for the polarization grating by summing, with the proper spatial phases, the contributions from the four component gratings. The results of such a calculation are shown in Fig. 8(a). The spatial dependence of the population transfer out of three of the eight ground state magnetic sublevels for excitation into the $P_{1/2}$ manifold of states is plotted; the results for the intensity grating are plotted as solid lines, while those for the polarization grating are dashed lines. Note that in the intensity grating, the spatial dependence of the population transferred is identical for each of the sublevels; the population transferred out of each of the five sublevels not included in the plot also exhibits this same spatial dependence. On the other hand, in the polarization grating the transfer from each sublevel has a different spatial dependence. Six separate gratings are formed in the magnetic sublevels with nonzero m_F. If the probe beam is resonant with a different transition than the excitation beams, it does not interact coherently with any excited state population, and the gratings formed in the individual ground state magnetic sublevels are the sole contributors to the signal. Thus it is necessary only to understand how the return of the excited state population to the ground state, whether through fluorescence or collisional decay, affects these gratings.

Figure 8(b) shows the spatial dependence of the total excited state population for the intensity grating (solid plot) and the polarization grating (dashed plot) under the same conditions as in Fig. 8(a). The excited state population in the intensity grating varies sinusoidally across the grating, exactly in phase with the population transferred out of each of the ground state magnetic sublevels. The excited state population in the polarization grating, however, is constant

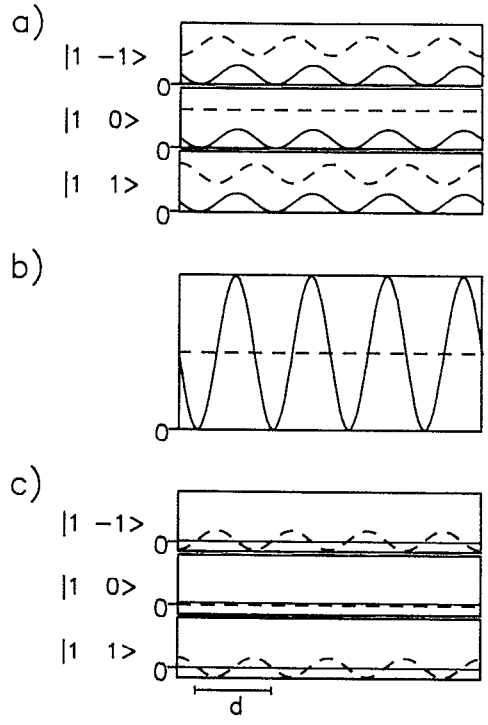

FIG. 8. (a) Spatial dependence of population transferred out of the three magnetic sublevels in the $F = 1$ ground state hyperfine line immediately after excitation. In all plots, the solid lines are for the intensity grating and the dashed lines are for the polarization grating. (b) Spatial dependence of the excited state population immediately after excitation under the same conditions as in (a). (c) Spatial dependence of population in magnetic sublevels of $F = 1$ ground state hyperfine level after complete, m_F-independent, excited-state quenching.

across the entire grating. There are two ways for this population to return to the ground state, collisional quenching and fluorescence; since the former mechanism is the dominant one in the flame experiments reported here, it is the only one we will consider.

We make the assumption that population in a particular excited state magnetic sublevel has an equal probability of being quenched into any of the ground state magnetic sublevels. This is reasonable, since quenching of the Na excited states is caused by a collisional transfer of energy to vibrational and rotational quanta of the collision partner (such as N_2). This assumption is borne out by comparison between theory and experiment.

In the intensity grating, the initial excited state population has the same spatial dependence as the population transferred out of each ground state magnetic sublevel; since the transfer out of and the relaxation back into each ground state sublevel is of the same magnitude, excited-state quenching eliminates the ground state gratings. On the other hand, the excited state population in the polarization grating does not vary across each fringe, and so equal quenching into all m_F levels can only add a constant amount of population (one-eighth of the initial excited state population) to each of these ground state gratings. Thus the population quenched from the excited state leaves the amplitudes of the ground state gratings unchanged.

Figure 8(c) shows the relative population loss from the same three ground state magnetic sublevels after complete excited state quenching; although the constant offsets in the polarization grating plots have changed, the sinusoidal gratings persist, and the quenching process does not contribute to the signal decay. Note that in the polarization grating plots in Fig. 8(c), the nulls of the $|1-1\rangle$ and $|1\,1\rangle$ magnetic sublevel gratings are actually below the "zero" level. This is indicative of optical pumping; population has been transferred from the peaks of the plots into the nulls of the plots due to the circularly polarized light in the grating decomposition.

We have thus shown that quenching collisions have no effect on the decay of Na polarization gratings. There is one more process to consider, however: collisions that scatter population among the ground state magnetic sublevels. For instance, it is evident from Fig. 8(c) that because the gratings in the $|1-1\rangle$ and $|1\,1\rangle$ magnetic sublevels are 180° out of phase, scattering between these states will cause both gratings to decay. In fact, scattering of population between any of the ground state gratings that are out of phase with one another will lead to the decay of the polarization grating signal. This is the process that is responsible for the nonzero intercept of Fig. 5.

We can also use a qualitative argument to understand why the polarization grating decays exhibit beats while the intensity grating decays do not. It can be shown theoretically[29] (as was first suggested by Rose *et al.*[16]) that the contributions of rcp and lcp intensity gratings to terms in the third-order polarization that oscillate at the ground state hyperfine splitting frequency are of opposite sign. A linearly polarized intensity grating can be thought of as the in-phase sum of an rcp and an lcp grating; thus the terms in the third-order polarization that oscillate at the ground state hyperfine splitting frequency cancel, and there are no beats in the intensity grating decay. In the polarization grating, the component rcp and lcp intensity gratings are spatially 180° out of phase, and so the hyperfine splitting terms add constructively, and the decay does contain beats.

Quantitative expressions for the grating signals using diagrammatic perturbation theory have been derived.[12,29] The TG experiment can, in general, be described by four double-sided Feynman diagrams.[31-37] Each four-wave mixing Feynman diagram corresponds to a three-dimensional integral containing material transition dipole matrix elements, each of the laser electric fields, and propagator terms that describe the evolution of the system. Each integral is evaluated and summed over all possible states, and the sum of the results is the third-order electric polarization. This material polarization in turn produces the signal field, whose functional form is found by multiplying the polarization by its complex conjugate. In this particular TG experiment, in which different excited state manifolds are involved in the excitation and probing steps, the number of diagrams is reduced to two; these are shown in Fig. 9. Also, the material response of interest is much slower than the laser pulses used, so we can make the simplifying assumption that the laser pulses and the signal are temporal delta functions, but with finite frequency bandwidths. This allows the integrals

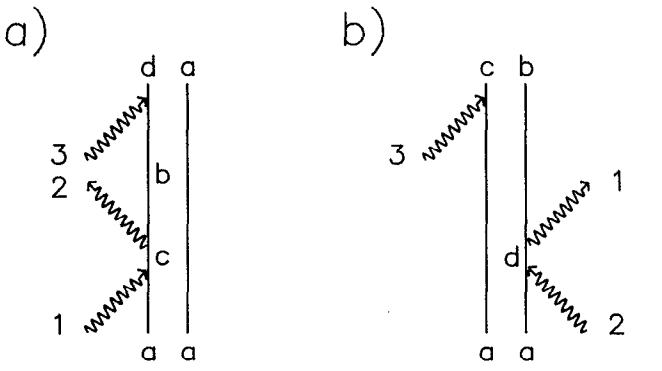

FIG. 9. The double-sided Feynman diagrams representing the two general processes that must be considered in the TG experiment in Fig. 4.

to be solved analytically. [The equations corresponding to Fig. 9(a) and Fig. 9(b) can be found in Ref. 29.]

Each of these integrals must also be summed over all of the relevant pathways through the states of the system. In this case, the states that must be used are the magnetic sublevels of the ground and excited states. Thus, all of the allowed four-step pathways through these 32 states must be found for each diagram. Trebino and Rahn showed that all of the two-step pathways from a particular ground state magnetic sublevel to another ground state magnetic sublevel through a given excited state manifold with given electric field polarizations at each step can be summed in advance in many cases.[18] Fourkas, Trebino, and Fayer generalized this concept in the form of an effective two-interaction matrix elements (ETIMEs). Using these ETIMEs, we can reduce the calculation in this experiment from 16 384 terms to 128; furthermore, many of these remaining terms are zero.

Taking the results of the qualitative analysis into consideration, we find (for times long enough that the $3P_{1/2}$ and $3P_{3/2}$ populations have equilibrated) an intensity grating signal given by

$$S(t) \propto \exp[-2(\Delta^2 D + 1/\tau)t], \tag{9}$$

where τ is the excited state lifetime (including the quenching contribution); thus Eq. (2) is recovered. The polarization grating signal under the same conditions is given by

$$S(t) \propto [43 + 60\cos(\omega_{21}t) + 25\cos(2\omega_{21}t)] \times \exp[-2(\Delta^2 D + 1/\tau_{21})t], \tag{10}$$

where ω_{21} is the ground state hyperfine splitting frequency and τ_{21} is the time for collisions that scatter population among the ground state hyperfine levels. Equation (10) shows oscillations at ω_{21} and at $2\omega_{21}$; the $2\omega_{21}$ oscillations appear as small peaks between the main peaks in the decays (see Fig. 4). The ratio of the ω_{21} and $2\omega_{21}$ amplitudes is accurately reproduced by this equation, without recourse to adjustable parameters. Note that the excited state lifetime does not appear in Eq. (10); this is consistent with the data, and it confirms the validity of the assumption that the m_F quantum number is randomized in excited-state quenching collisions. Furthermore, without the qualitative information about the decay processes provided by the GDM analysis of

this problem, there would be no way to distinguish the decay constants in Eqs. (9) and (10); these constants are incorporated into diagrammatic perturbation theory in a purely phenomenological manner.

From Eq. (9) it can be seen that if the excited state quenching rate is great enough and the diffusion rate small enough, the intensity grating decay will be independent of fringe spacing over a large range of fringe spacings. On the other hand, for the fringe spacings studied here, the rate of collisions that scatter population among the ground state magnetic sublevels is much slower than the quenching collision rate. If the hyperfine scattering rate is slow enough, it is clear from Eq. (10) that the polarization grating decay time will be sensitive to fringe spacing.

VI. CONCLUDING REMARKS

The polarization-selective transient grating is a powerful tool for probing subnanosecond time scale combustion dynamics. It is a zero-background experiment, and therefore excellent signal-to-noise ratios can be achieved. It is relatively insensitive to reabsorption, and is capable of making sub-Doppler, high resolution spectroscopic measurements. In addition, the TG technique is sensitive to transport over micron distance scales, and areas with a diameter as small as a few tens of microns or as large as many millimeters can be probed. Using this one technique, we have been able to study four sorts of collisions of Na atoms: diffusional, excited-state quenching, excited-state population scattering, and ground state population scattering (the last of which, to our knowledge, had never been studied in flames previously). Even in a fairly unstable flame, we are able to measure all of these numbers with significant precision; in fact, the major source of uncertainty in the measurements is the temperature at the point in the flame at which we are making the measurements. Furthermore, the grating decomposition method and ETIMEs are especially useful in creating and simplifying theoretical models of experiments such as these. By going to very small fringe spacing, the TG technique should be able to measure local velocity distributions and therefore translational temperatures [see Eq. (1)]. The TG technique promises to be useful in the study of the dynamics of intrinsic combustion species, as well as in the study of other gas-phase systems and plasmas.

ACKNOWLEDGMENTS

This work was supported in part by the Office of Naval Research, Physics Division, Grant No. N000014-89-J1119. Computing equipment was provided by the National Science Foundation, Grant No. CHE 99-21737. J. F. thanks the National Science Foundation for a graduate fellowship. We thank Dr. Mark A. Dugan and Dr. Rick Trebino for helpful discussions.

[1] J. Glassman, *Combustion*, 2nd ed. (Academic, Orlando, 1987).
[2] A. C. Eckbreth, G. M. Dobbs, J. H. Stufflebeam, and P. A. Tellex, Appl. Opt. **23**, 1328 (1984).
[3] B. Attal-Tretout and P. Bouchardy, La Rech. Aerosp. **5**, 19 (1987).
[4] D. R. Crosley, Comb. Flame **78**, 153 (1989).
[5] K. Kohse-Höinghaus, Appl. Phys. B **50**, 455 (1990).
[6] P. Ewart and S. V. O'Leary, Opt. Lett. **11**, 279 (1986).
[7] P. Ewart, P. Snowdon, and I. Magnusson, Opt. Lett. **14**, 563 (1989).
[8] T. Dreier and D. J. Rakestraw, Opt. Lett. **15**, 72 (1990).
[9] T. Dreier and D. J. Rakestraw, Appl. Phys. B **50**, 479 (1990).
[10] D. J. Rakestraw, R. L. Farrow, and T. Dreier, Opt. Lett. **15**, 709 (1990).
[11] H. J. Eichler, P. Günter, and D. W. Pohl, *Laser-Induced Dynamic Gratings* (Springer, Berlin, 1986).
[12] J. T. Fourkas, T. R. Brewer, H. Kim, and M. D. Fayer, Opt. Lett. **16**, 177 (1991).
[13] A. von Jena and H. E. Lessing, Opt. Quant. Electron. **11**, 419 (1979).
[14] G. Eyring and M. D. Fayer, J. Chem. Phys. **81**, 4314 (1984).
[15] T. S. Rose, W. L. Wilson, G. Wäckerle, and M. D. Fayer, J. Phys. Chem. **91**, 1704 (1987).
[16] T. S. Rose, W. L. Wilson, G. Wäckerle, and M. D. Fayer, J. Chem. Phys. **86**, 5370 (1987).
[17] R. J. Kneisler, F. E. Lytle, G. J. Fiechtner, Y. Jiang, G. B. King, and N. M. Laurendeau, Opt. Lett. **14**, 260 (1989).
[18] R. Trebino and L. A. Rahn, Opt. Lett. **12**, 912 (1987).
[19] L. A. Rahn and R. Trebino, in *Advances in Laser Science—III*, edited by A. C. Tam, J. L. Gole, and W. C. Stwalley (American Institute of Physics, New York, 1988), p. 272.
[20] B. P. Kibble, G. Koppley, and L. Krause, Phys. Rev. **153**, 9 (1967).
[21] A. F. Ashton and A. N. Hayhurst, Trans. Faraday Soc. **69**, 652 (1972).
[22] R. E. Russo and G. M. Hieftje, Appl. Spectrosc. **36**, 92 (1982).
[23] Y. Takubo, T. Okamoto, and M. Yamamoto, Appl. Opt. **25**, 740 (1986).
[24] A. J. Alfano, Appl. Opt. **28**, 5010 (1989).
[25] J. R. Barker and R. E. Weston, Jr., J. Chem. Phys. **65**, 1427 (1976).
[26] K. C. Smyth, P. K. Schenck, and W. G. Mallard, in *Laser Probes for Combustion Chemistry*, ACS Symposium Series No. 134, edited by D. R. Crosley (American Chemical Society, Washington, D.C., 1980), p. 175.
[27] P. W. Atkins, *Physical Chemistry*, 3rd ed. (W. H. Freeman, New York, 1986).
[28] L. Ebdon, *Atomic Absorption Spectroscopy* (Heydon, London, 1982).
[29] J. T. Fourkas, R. Trebino, and M. D. Fayer, J. Chem. Phys. (submitted).
[30] M. D. Levenson and S. S. Kano, *Introduction to Nonlinear Spectroscopy*, Rev. ed. (Academic, San Diego, 1988).
[31] L. J. Rothberg and N. Bloembergen, Phys. Rev. A **30**, 820 (1984).
[32] T. K. Yee and T. K. Gustafson, Phys. Rev. A **18**, 1597 (1978).
[33] Y. Prior, IEEE J. Quant. Electron. **QE-20**, 37 (1984).
[34] J. Bordé and Ch. J. Bordé, J. Mol. Spectrosc. **78**, 353 (1979).
[35] J. G. Fujimoto and T. K. Yee, IEEE J. Quant. Electron. **QE-19**, 861 (1983).
[36] J. G. Fujimoto and T. K. Yee, IEEE J. Quant. Electron. **QE-22**, 1215 (1986).
[37] P. Ye and Y. R. Shen, Phys. Rev. A **25**, 2183 (1982).